AIP | Review of Scientific Instruments

Design and analysis of a spectro-angular surface plasmon resonance biosensor operating in the visible spectrum

Sandrine Filion-Côté, Philip J. R. Roche, Amir M. Foudeh, Maryam Tabrizian, and Andrew G. Kirk

Citation: Review of Scientific Instruments **85**, 093107 (2014); doi: 10.1063/1.4894655
View online: http://dx.doi.org/10.1063/1.4894655
View Table of Contents: http://scitation.aip.org/content/aip/journal/rsi/85/9?ver=pdfcov
Published by the AIP Publishing

Design and analysis of a spectro-angular surface plasmon resonance biosensor operating in the visible spectrum

Sandrine Filion-Côté,[1,2,a)] Philip J. R. Roche,[1] Amir M. Foudeh,[2] Maryam Tabrizian,[2,3] and Andrew G. Kirk[1]

[1]*The Photonic Systems Group, Dept. Electrical and Computer Engineering, McGill University, McConnell Engineering Building, Montréal H3A 0E9, Canada*
[2]*Department of Biomedical Engineering, McGill University, Duff Medical Building, Montréal H3A 2B4, Canada*
[3]*Faculty of Dentistry, McGill University, Strathcona Anatomy & Dentistry Building, Montréal H3A 0C7, Canada*

(Received 12 June 2014; accepted 24 August 2014; published online 23 September 2014)

Surface plasmon resonance (SPR) sensing is one of the most widely used methods to implement biosensing due to its sensitivity and capacity for label-free detection. Whilst most commercial SPR sensors operate in the angular regime, it has recently been shown that an increase in sensitivity and a greater robustness against noise can be achieved by measuring the reflectivity when varying both the angle and wavelength simultaneously, in a so-called spectro-angular SPR biosensor. A single value decomposition method is used to project the two-dimensional spectro-angular reflection signal onto a basis set and allow the image obtained from an unknown refractive index sample to be compared very accurately with a pre-calculated reference set. Herein we demonstrate that a previously reported system operated in the near infra-red has a lower detection limit when operating in the visible spectrum due to the improved spatial resolution and numerical precision of the image sensor. The SPR biosensor presented here has an experimental detection limit of 9.8×10^{-7} refractive index unit. To validate the system as a biosensor, we also performed the detection of synthetic RNA from pathogenic *Legionella pneumophila* with the developed biosensing platform. [http://dx.doi.org/10.1063/1.4894655]

I. INTRODUCTION

Surface plasmon resonance (SPR) is one of the most widely used transduction mechanisms for biosensing.[1] Biosensors are essential devices in the biomedical, environmental, and agricultural fields since they allow the monitoring of vital information required to diagnose diseases and detect the presence of contaminants in water and soil. Surface plasmons are charge-density oscillations that exist at the interface of two media and propagate on that interface. The propagating conditions of the surface plasmons are highly dependent on the refractive index of the medium adjacent to the metal film which makes it a powerful method to track changes in the refractive index of a sample due to binding events and it is therefore highly useful for biosensing.

SPR-based biosensors can be used in an extensive range of applications and they are particularly very attractive for medical diagnosis and environmental monitoring due to their ability to perform label free measurement in real time. In addition, the metal surface can be functionalized to specifically capture any target molecules to investigate the interaction between an analyte and its ligand[2] required for the detection of major diseases.[3] Since these measurements can also be performed with gaseous samples[4] SPR-based biosensors are valuable resources for environmental samples monitoring such as air quality. In more recent years, the application of SPR-based biosensors has been extended for whole cell detection and an increasing amount of research is being conducted on the subject.[5,6] This approach provides us with advantage of reducing the number of steps required by extracting genetic materials of cells such as DNA, RNA or other cell sub-components by detecting them directly on the sensing surface. Additionally, these sensitive biosensors are also very useful for the characterisation of thin films[7,8] since the SPR response does not only depend on the refractive index of the material adjacent to the metal but also on its thickness. The characterisation of thin films is important for the development of film deposition methods, for the design of appropriate biomaterials and multilayer structures, for the assessment of biofilm formation and for the interactions of thin films with various analytes. While not exhaustive, these examples provide an overview of the wide range of applications that SPR biosensors cover and stress the need for high resolution SPR-based biosensors.

There are multiple known architectures to excite surface plasmons. The conventional approach is to measure the intensity of the reflected light versus either the incident angle or wavelength as shown in Figures 1(a) and 1(b). In this design, the refractive index of a sample can be extracted by tracking the resonant angle or wavelength of the resulting SPR curve[9] (Figure 1(c)). A new approach that has shown potential is to obtain the complete dispersion curve for both the wavelength and the angular channels simultaneously. This can be

a)Author to whom correspondence should be addressed. Electronic mail: sandrine.filioncote@mail.mcgill.ca.

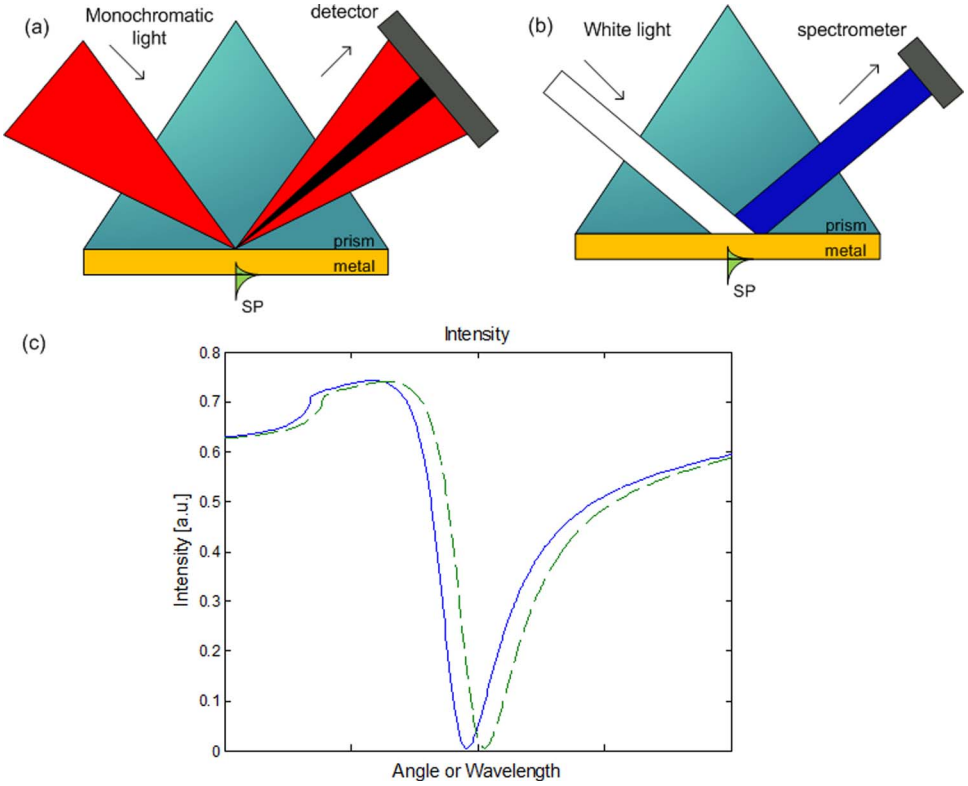

FIG. 1. Angular (a) and wavelength (b) interrogation; (c) SPR curves for two different refractive indices.

achieved by using a white light source that is focused with a cylindrical lens onto the surface. The reflected spectrum is re-collimated using a second cylindrical lens in order to obtain the angular spectrum whilst being simultaneously dispersed along the orthogonal (wavelength) axis using a diffraction grating. The resulting two-dimensional intensity distribution is captured onto a two-dimensional detector array,[10] as shown in Figure 2.

The advantage of the spectro-angular SPR image over a conventional SPR curve is the possibility to use image processing tools to extract the information about changes in the refractive index of the sample rather than relying on dip-finding algorithms. The analysis method developed for the spectro-angular SPR biosensor is referred to as the double projection method (DPM).[11] This method consists in creating a basis set of SPR images through single-value decomposition and evaluating each new image using this basis to extract the refractive index of the sample. It has previously been shown that this method depends greatly on both the resolution of the camera and even more significantly on the bit depth of the data acquisition.[11]

A spectro-angular SPR system built in our laboratories with a light source at 850 nm and the detection limit of the system, 1.5×10^{-6} RIU, was found to be close to the predicted detection limit for the camera resolution and bit depth.[10] In order to improve the detection limit of the SPR biosensor, we sought to employ image sensors with greater bit depth and more pixels. This could be achieved by choosing a wavelength for the light source in the visible spectrum since the cameras operating in this range have much higher resolution and bit depth than the cameras in the infrared. The simulation results performed at 630 nm with available visible camera parameters presented in this paper are a demonstration of the potential improvement of the limit of detection.

II. COMPARISON OF VISIBLE AND INFRARED SPECTRA

Light sources in the infrared spectrum, namely at 850 nm, are often chosen to implement SPR biosensors since the SPR resonance curve is narrower at these wavelengths than in the visible spectrum, therefore facilitating the evaluation of the resonant angle (Figure 3). Using the parameters described in the figure caption, the full widths at half maximum (FWHM) of the SPR curves are 3.35° and 0.65° for 630 nm and 850 nm, respectively. However, when the sensitivity (S), i.e., the shift in the resonant angle with respect to the change in refractive index is considered, it is larger at 630 nm than at 850 nm with sensitivities of 74°/RIU (RIU: refractive index units) compared to 59°/RIU, respectively. If both parameters are simultaneously taken into account by calculating the commonly used figure of merit (FOM)[12] shown in Eq. (1), the conventional SPR biosensors have a higher FOM in the infrared than in the visible (91 RIU^{-1} at 850 nm as compared to 22 RIU^{-1} at 630 nm, for example).

$$FOM = \frac{S}{FWHM} = \frac{\Delta^{\circ}/\Delta RI}{FWHM} \; OR \; \frac{\Delta\lambda/\Delta RI}{FWHM}. \qquad (1)$$

We next investigated the impact of the choice of input wavelength on the performance of the spectro-angular SPR biosensor. The details of the DPM method are described in Alleyne *et al.*[11] Briefly, this method employs a set of

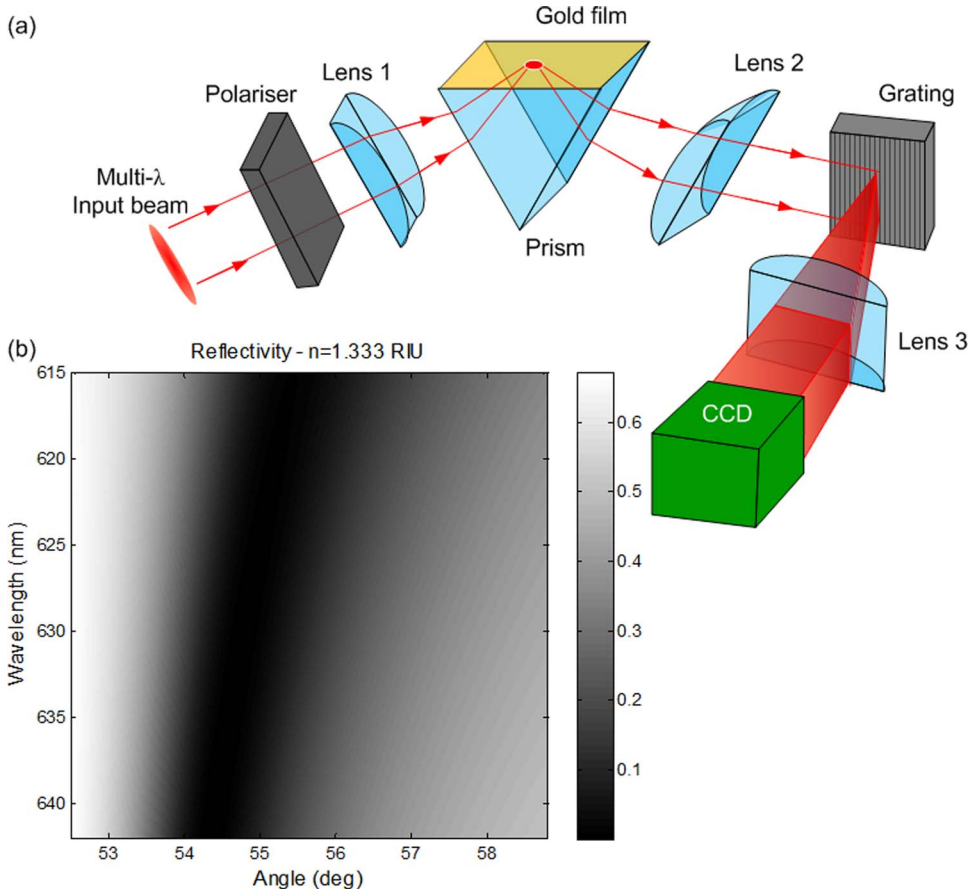

FIG. 2. (a) Spectro-angular interrogation and (b) spectro-angular SPR image.

simulated SPR images corresponding to multiple refractive indices across the dynamic range of the biosensor and comparing the experimental images with the simulated images to estimate the unknown refractive indices. The first step consists in simulating the reflection images of known refractive indices and grouping them in a matrix. Singular value decomposition (SVD) is applied on the matrix and the first projection is performed; the matrix of reflection images is projected on the SVD processed matrix to obtain the basis set. With the basis set in memory, every image of unknown refractive index is rearranged into a column vector and is projected against the SVD processed matrix creating a weight vector. The weight vector is then projected against each row in the basis set and the unknown refractive index is estimated with high precision by finding the maximum point from the resulting vector using interpolation.

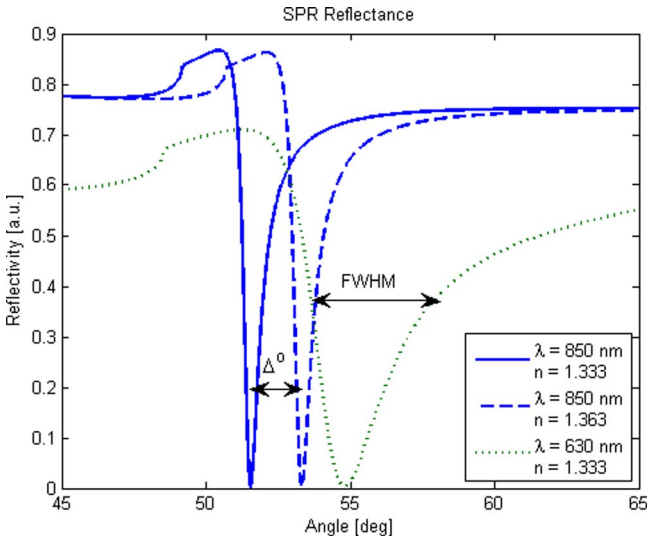

FIG. 3. SPR curves for wavelengths of 850 nm and 630 nm. The following common parameters were used: layers of 2.3 nm of titanium and 46.9 nm of gold on SF11 glass (1.7789 RIU) with sample of 1.333 RIU and 1.363 RIU.

As mentioned earlier, the performance of the DPM depends greatly on the bit depth of the analog-to-digital converter (ADC) and the number of pixels of the camera. To validate the choice of wavelength for the light source, simulations have been performed to compare the theoretical detection limit at two center wavelengths, 630 nm and 850 nm, for various camera parameters. The root-mean-square (RMS) errors for the estimation of refractive index changes are calculated for both wavelengths using Matlab. In the first simulation, the same acquisition parameters are used at both wavelengths: a spatial resolution of 1024 × 1024, a 16-bit ADC. In both cases the basis set is derived from 51 images representing refractive index from 1.30 to 1.35 RIU, therefore with an interval of 0.001 RIU. The test images are chosen to represent the worst-case scenario which is when the test images correspond to refractive indices lying between the refractive indices of the basis images. Equation (2) shows the main test set, n^t. Three other test sets of images, n^{tt}, are create to estimate different changes in refractive index, $\Delta = 10^{-6}$, 10^{-7},

TABLE I. RMS estimation error for different refractive index changes using the same acquisition parameters (1024 × 1024 resolution, 16-bit ADC).

	RMS estimation error (no noise)		RMS estimation error (4-bit noise)		RMS estimation error (5-bit noise)	
RI change (Δ) (RIU)	630 nm	850 nm	630 nm	850 nm	630 nm	850 nm
10^{-6}	1.414×10^{-9}	7.211×10^{-9}	8.718×10^{-9}	9.798×10^{-9}	2.248×10^{-8}	1.363×10^{-8}
10^{-7}	1.414×10^{-9}	2.449×10^{-9}	8.000×10^{-9}	7.211×10^{-9}	2.067×10^{-8}	1.240×10^{-8}
10^{-8}	7.094×10^{-17}	7.094×10^{-17}	9.695×10^{-9}	6.928×10^{-9}	2.104×10^{-8}	1.172×10^{-8}

and 10^{-8}, with respect to the main test set. Equation (3) gives an example of n^{tt} with $\Delta = 10^{-6}$.

$$n_k^t = \begin{cases} 1.3005 \\ 1.3015 \\ \quad \vdots \\ 1.3495 \end{cases}, \tag{2}$$

$$n_k^{tt} = \begin{cases} 1.300501 \\ 1.301501 \\ \quad \vdots \\ 1.349501 \end{cases}, \tag{3}$$

The refractive index change is estimated for each image in the sets and the estimation error is calculated. The RMS error is then used to compare the performance at both wavelengths.

$$\delta_k = \left|\left(\hat{n}_k^{tt} - \hat{n}_k^t\right) - \Delta\right|, \tag{4}$$

$$\delta_{RMS} = \sqrt{\sum_k \frac{\delta_k^2}{N}} = \sqrt{\sum_k \frac{\left|\left(\hat{n}_k^{tt} - \hat{n}_k^t\right) - \Delta\right|^2}{N}}. \tag{5}$$

δ_k is the kth estimation error, δ_{RMS} is the RMS error, $\hat{n}_k$ is the kth estimated refractive index, and N is the number of images in the test set which in this case is 50. Table I shows the simulation results. Any results in the order of 10^{-16} or 10^{-17} should be considered zero as it is due to the finite numerical precision of Matlab. The results shown with "4-bit noise" and "5-bit noise" are the RMS estimation error when the test images were modified to add Gaussian noise with a standard deviation of $2^{Nb-1}/2^n - 1$ where N_b is the number of bits of noise (4 and 5 bits in this case) and n is the number of bit in the ADC (16-bit in this case). The noise is added to simulate experimental conditions. The results presented in Table I demonstrate that changing the wavelength of the light source will not significantly change the precision of the refractive index measurement. In other words, the broader SPR curve at 630 nm does not degrade the refractive index estimation with the DPM.

The second simulation for the comparison between 630 nm and 850 nm is to use different acquisition parameters. In the case of 850 nm, the camera has a resolution of 480 × 640 and uses a 10-bit ADC. Those parameters correspond to the camera that was used in a previous experimental system. For the 630 nm case, the camera has a resolution of 1024 × 1024 and uses a 14-bit ADC. The RMS errors shown in Table II indicate that the detection limit should improve upon using a camera and a light source operating in the visible spectrum. The theoretical resolution is 14 times and 16 times higher with the new parameters for 4 bits of noise and for 5 bits of noise, respectively. This suggests that it will be possible to detect smaller refractive index changes than the previous system which had an experimentally determined detection limit of 1.5×10^{-6} RIU.

III. EXPERIMENTAL RESULTS

In the current experimental system shown in Figure 2, the light source is an LED centered at 630 nm with a full width at half maximum of 17.9 nm and an output power of 5.2 mW. Lenses with focal length of 75 mm and a diameter of 25 mm are used to focus and re-collimate the beam before and after the reflection on the sensing surface. The combination of the focusing lens and the glass prism that has a refractive index of 1.78 at 630 nm creates an angular spectrum of 8° on the gold surface. This angular spectrum allows a dynamic range of 0.07 RIU. The coupling prism was an SF11 equilateral triangular prism and the thin metal film used a 2.3 nm Titanium adhesion layer with a 46.9 nm gold layer. To disperse the wavelengths of the beam onto the camera, a reflective diffraction grating with 1800 grooves per mm and a cylindrical lens with a focal length of 150 mm were used. The cameras are Pike F-421B from Allied Vision Technology.

One of the main challenges of SPR biosensors is to minimise thermal noise and temperature drift. The rise in the temperature of the sample is due to the light beam incident on

TABLE II. RMS estimation error for different refractive index changes using different acquisition parameters (630 nm: 1024 × 1024, 14-bit ADC; 850 nm: 480 × 640, 10-bit ADC).

	RMS estimation error (no noise)		RMS estimation error (4-bit noise)		RMS estimation error (5-bit noise)	
RI change (Δ) (RIU)	630 nm	850 nm	630 nm	850 nm	630 nm	850 nm
10^{-6}	1.147×10^{-16}	3.397×10^{-8}	3.924×10^{-8}	5.804×10^{-7}	8.290×10^{-8}	1.352×10^{-6}
10^{-7}	1.549×10^{-16}	1.273×10^{-8}	4.264×10^{-8}	5.623×10^{-7}	8.356×10^{-8}	1.304×10^{-6}
10^{-8}	7.094×10^{-17}	4.810×10^{-9}	4.308×10^{-8}	6.878×10^{-7}	8.890×10^{-8}	1.331×10^{-6}

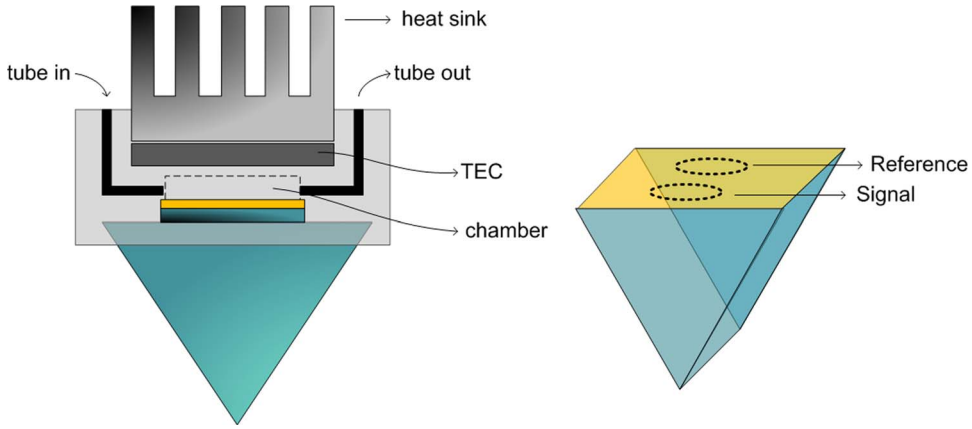

FIG. 4. (Left) Prism holder, fluidic system, and TEC. The chamber for the second channel is behind the one shown. (Right) Top view of the gold coated prism showing the position of the two chambers.

the gold surface and the plasmon propagating on the metal-dielectric interface. As temperature increases, the density of a liquid decreases causing a decrease in refractive index. For example, water has a refractive index of 1.3321 RIU at 630 nm at 21.5 °C[13] and as temperature increases, its refractive index decreases by 94.3×10^{-6} RIU/°C.[13] Two techniques are used in this work to reduce the noise associated with temperature change: a thermoelectric cooler (TEC) and a reference channel (Figure 4). A TEC controller from Wavelength Electronics with a linear temperature stability of 0.03 °C was used. The temperature controller prevents the temperature from largely varying over the time of the acquisition. To deal with the remaining fluctuations due to the limited precision of the TEC and the other sources of noise, such as the power fluctuations in the light source and the background light, a reference channel sharing common parameters with the signal channel was implemented. The input light source was divided in two with a fibre coupler to allow that each beam traverses identical optical components. Although each channel had its own chamber for the sample, the temperature controller was common for both light trajectories. At the output, two identical cameras were acquiring the signals simultaneously. To remove undesired artefacts created by the optical system, the images obtained from each channel were normalised before being analysed. As such, any noise resulting from the optical components could be removed with this normalisation. The normalisation was performed by dividing the image to be analysed with an image that does not exhibit a drop in intensity from the excitation of a surface plasmon but shares the undesired artefacts. The latter image was obtained prior to introducing the buffer in the system when the chamber was filled with air and no surface plasmon was excited since the parameters of the system were optimised for the buffer. The other advantage of normalisation was to reduce the effect of the Gaussian distribution of the input spectrum since the simulation performed for the basis set assumes a flat spectrum.

Figure 5 shows the real-time refractive index estimation of a sample. In this case, water was flowing in both the signal and reference channels and samples of salt water of various concentrations were also introduced in the signal channel only. The resolution of a biosensor is generally defined as the smallest measurable signal and is calculated using the standard deviation of the output noise.[14] Refractive index changes smaller than the standard deviation would be lost in the noise floor. To determine the detection limit of our system, the standard deviation was calculated on a set of data corresponding to the signal generated when buffer solution was flowing through the system over a time internal of 2 min and a detection limit of 9.8×10^{-7} RIU was obtained.

To validate this platform as a biosensor, a calibration curve was first obtained using a dilution series of salt concentration in distilled water from 500 mM, 250 mM, 100 mM, 62.5 mM, 50 mM, 25 mM, and 10 mM, corresponding to theoretical refractive index changes (with respect to distilled water) of 5.04×10^{-3} RIU, 2.56×10^{-3} RIU, 1.03×10^{-3} RIU, 6.46×10^{-4} RIU, 5.17×10^{-4} RIU, 2.59×10^{-4} RIU, and 1.04×10^{-4} RIU,[15] respectively. Figure 6 shows the linear

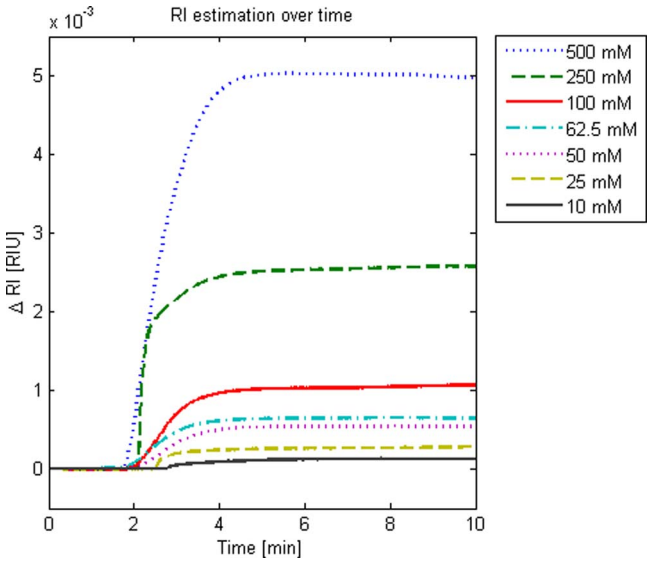

FIG. 5. Refractive index estimation in real-time. The refractive index changes performed using salt water are 1.80×10^{-5} RIU, 8.85×10^{-5} RIU, 3.58×10^{-4} RIU, 8.93×10^{-4} RIU, and 1.78×10^{-3} RIU.

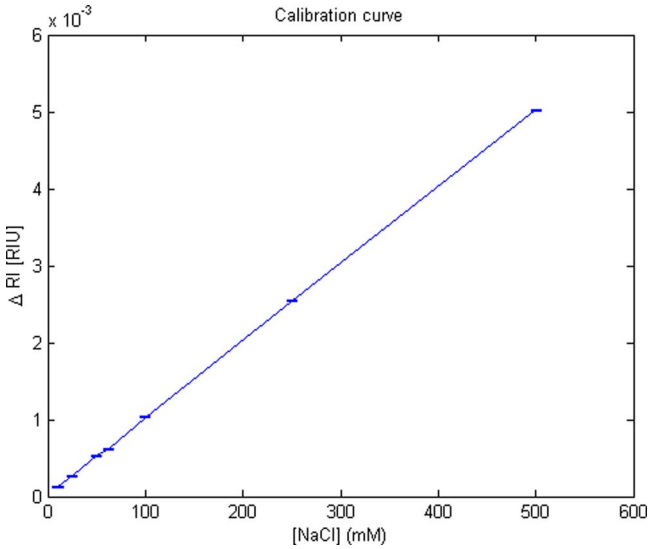

FIG. 6. Calibration curve of the spectro-angular SPR biosensor.

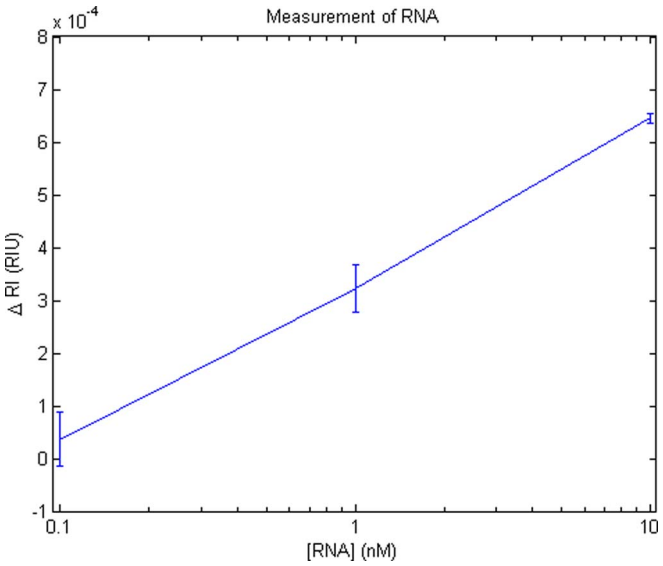

FIG. 7. Measurement of three different concentrations of RNA from *Legionella pneumophila* with the spectro-angular SPR biosensor.

relationship between the refractive index change and the concentration of salt in the solution. The measured refractive index changes with respect to the theoretical refractive index changes have an R-squared value of 0.9999 further confirming that the system performs accurate measurements. It is important to mention that these measurements report on changes of refractive indices and not on their absolute values. The absolute values of refractive indices might be measured with much more complicated systems calibration and through a more accurate control of the temperature.

The next step was to perform a relevant bioassay to demonstrate the applicability of the system for diagnostic purposes and more specifically for water quality management. A synthetic RNA sequence from *Legionella pneumophila*'s 16s rRNA was used.[3] *L. pneumophila*, found in most engineered water sources, are pathogenic bacteria causative of legionellosis, a severe and life-threatening pneumonia.[16] To detect *L. pneumophila's* target RNA, a detection system based on capture and detector probes specificity, and quantum dots (QD) SPR signal amplification was utilized.[3] The gold surface of the sensor was first functionalized with thiol-modified DNA capture probes complementary to the target RNA.[3] Following the immobilization, substrates were treated with 1 mM MCH to control the probe orientation. The surface was passivated with 2.5X Denhardt blocking agent to minimize non-specific binding. The *L. pneumophila* RNA samples were then mixed with biotinylated detector probes and flowed to the chamber at three different concentrations ranging from 100 pM, 1 nM to 10 nM, followed by the introduction of streptavidin-conjugated quantum dots with emission wavelength at 800 nm for signal amplification.[17] The QD signal amplification strategy was required to proportionally increase the refractive index shift generated by the sample improving the signal to noise ratio. Figure 7 shows the refractive index shifts as a function of RNA sample concentration demonstrating the ability of the proposed SPR-based biosensor platform to perform relevant biological bioassays.

IV. CONCLUSION

We have demonstrated a spectro-angular surface plasmon resonance biosensor operating in the visible spectrum. We presented experimental results demonstrating that the system works properly and accurately measures changes of refractive index in real-time. We additionally demonstrated that the biosensor is capable of performing biologically relevant bioassays by detecting different concentrations of RNA from *Legionella pneumophila*. Our simulations predict that a system operating in the visible spectrum with a higher spatial resolution and a higher bit depth has a superior performance than a system working in the infrared (9.8×10^{-7} RIU versus 1.5×10^{-6}), although having an inferior FOM for its SPR curve. The experimental detection limit of the previous biosensor operating in the infrared matched its predicted value. Considering the same amount of noise (5-bit), the predicted detection limit for the new biosensor operating in the visible spectrum was 8.3×10^{-8} RIU, 10 times higher than commercially available Biacore SPR biosensors with a detection limit of 10^{-7} RIU.[14] The discrepancy between our simulation and experimental results is most likely due to thermal noise. The next step in this project is to reduce the thermal noise and improve the drift cancellation by managing more adequately the reference channel to further improve the detection limit of the biosensor and obtain results closer to the theoretical detection limits.

ACKNOWLEDGMENTS

The authors would like to acknowledge support from the Fonds de recherche du Québec - Nature et technologies, the Natural Sciences and Engineering Research Council of Canada, the Faculty of Engineering of McGill University and the NSERC-CREATE Training Program in Integrated Sensor Systems.

[1]J. Homola, Chem. Rev. **108**, 462 (2008).
[2]T. Xue *et al.*, Biosens. Bioelectron. **58**, 374 (2014).

[3]A. M. Foudeh *et al.*, Biosens. Bioelectron. **52**, 129 (2014).
[4]A. Berrier *et al.*, Sensor Actuators, B **160**, 181 (2011).
[5]V. Chabot *et al.*, Biosens. Bioelectron. **24**, 1667 (2009).
[6]Ö. Torun *et al.*, Biosens. Bioelectron. **37**, 53 (2012).
[7]Z. Ozbek, M. Erdogan, and R. Capan, Sensor Actuators, B **196**, 328 (2014).
[8]Y. W. Fen and W. M. M. Yunus, AIP Conf. Proc. **1482**, 132 (2012).
[9]A. Shalabney and I. Abdulhalim, Opt. Lett. **37**(7), 1175 (2012).
[10]C. J. Alleyne, P. J. R. Roche, S. Filion-Côté, and A. G. Kirk, Opt. Lett. **36**, 46 (2011).
[11]C. J. Alleyne, A. G. Kirk, W.-Y. Chien, and P. G. Charette, Opt. Express **16**, 19493 (2008).
[12]H. Jiandong and Z. Xiangyang, Symp. Photonics Optoelectron. **5230137**, 1 (2009).
[13]M. Daimon and A. Masumura, Appl. Opt. **46**, 3811 (2007).
[14]M. Piliarik and J. Homola, Opt. Express **17**, 16505 (2009).
[15]See http://us.mt.com/us/en/home/supportive_content/application_editorials/Sodium_Chloride_re_e.html for refractometry concentration table - Sodium Chloride, Mettler Toledo.
[16]M. Swanson and B. Hammer, Annu. Rev. Microbiol. **54**, 567 (2000).
[17]L. Malic, M. G. Sandros, and M. Tabrizian, Anal. Chem. **83**, 5222 (2011).